Supplementary Information for

Linking Long-range Surface-Induced Mobility Enhancement and Fragility in Polymer Glasses

Haoran Nie[1†], Xiwen Chen[1,2†], Xiyue Li[1], Zongyi Ma[1], Rui Zhang[1,2,3,4*], and Ophelia K. C. Tsui[1,2*]

*Corresponding authors. Email: okctsui@ust.hk and ruizhang@ust.hk

† These authors contributed equally to this work.

This file includes:

Supplementary Note
Supplementary Figs. 1 to 10
Supplementary Tables 1 to 2
Supplementary References

Supplementary Note

1. Heaviside-step model for the τ(z) profile of freestanding polymer films

We model the relaxation times for freestanding polymer films using a layer model, where the relaxation time near the two free surfaces (τ_{surf}) is significantly shorter than the that in the interior (τ_0) sandwiched in the middle. As depicted in Fig. 1c, if we assume that the molecular dynamics in each region are homogeneous and that the thickness of each surface region is h_{t}, the layer model for $\tau(z)$ of freestanding films with thickness $h > 2h_{\mathrm{t}}$ is expressed as,

$$\tau(z) = \tau_{\mathrm{surf}} + H(z - h_{\mathrm{t}}^{\mathrm{nano}}) \cdot (\tau_0 - \tau_{\mathrm{surf}}) - H(z - h + h_{\mathrm{t}}^{\mathrm{nano}}) \cdot (\tau_0 - \tau_{\mathrm{surf}}), \quad (1)$$

where $H(z')$ represents the Heaviside-step function, equal to zero when $z' < 0$ and one when $z' > 0$. For a freestanding film with thickness h, the average relaxation time τ_{film} is evaluated through linear arithmetic averaging:

$$\tau_{\mathrm{film}}(h) = \frac{1}{h}\int_0^h \tau(z)dz. \quad (2)$$

2. Mapping ratios of PMMA, PS and PVC in simulation

The determination of the mapping ratio for coarse-grained (CG) models of different polymers follows the protocol proposed by Kwansa et al. [1]. For PVC, PS and PMMA, the corresponding monomers consist of 6, 16, and 15 atoms respectively. Excluding hydrogen atoms—which contribute minimally to mass and are less relevant to molecular dynamics in systems without hydrogen bonding—we find that the effective atom counts are 3, 8, and 7 for PVC, PS, and PMMA, respectively.

For the systems including both backbone (A) and side-group (B) beads, i.e., PS and PMMA, the mapping ratio is defined as the ratio of the number of heavy atoms (excluding hydrogen) to the number of CG beads: 4:1 for PS and 3.5:1 for PMMA. In the case of PVC, if we use two CG beads, the mapping ratio becomes 1.5:1, which is significantly lower than those for PS and PMMA. This indicates that the degree of coarse graining is too high for PVC. Consequently, we used a single CG bead to represent the whole PVC monomer, yielding a mapping ratio of 3:1. The ratio is comparable to that of PS and PMMA, indicating similar degrees of coarse-graining across these polymers (Supplementary Table 2).

3. Determination of T_{g} and fragility for different polymers from CG-MD simulations

To compute the fragility (m) of the polymers, a bulk model without free surfaces was constructed for PMMA, PS and PVC, with an example for PS shown in Supplementary Fig. 6a. This model consists of 50 chains, each containing 200 monomers, with periodic boundary conditions applied in all dimensions. The initial configuration was generated using a random walk algorithm and equilibrated at 300 K following the method described by Hsu and co-workers (see Refs. 41 and 50 in the main text). After equilibrium, the system was heated to higher temperatures T. At each T, equilibration was performed for 10 ns, during which physical quantities such as atomic positions ($\mathbf{r}$) were recorded every 0.4 ns. To determine the

glass transition temperature (T_g), we first computed the self-part of the intermediate scattering function, F_s:

$$F_s(\mathbf{q},t) = \frac{1}{N}\sum_j^N \left\langle \exp\left[-i\mathbf{q}\cdot\left(\mathbf{r_j}(t)-\mathbf{r_j}(0)\right)\right]\right\rangle, \quad (3)$$

where $\mathbf{r_j}$ is the position of the j^{th} atom and $\mathbf{q}$ is the first peak of the structure factor, $S(\mathbf{q})$, which is defined by

$$S(\mathbf{q}) = \frac{1}{N}\sum_{j=1}^N \sum_{k=1}^N \exp\left[-i\mathbf{q}\cdot\left(\mathbf{r_j}-\mathbf{r_k}\right)\right]. \quad (4)$$

Here, the magnitude of $\mathbf{q}$ was fixed at 15.19 nm^{-1} in the x-direction, with variations in either the magnitude or direction having an insignificant effect on the results. The structural relaxation time (τ) for each temperature T (Supplementary Fig. 6b) is defined as the time at which $F_s(\mathbf{q},\tau) = 0.2$. All results for $\tau(T)$ are fitted to the Vogel-Fucher-Tammann (VFT) equation [2]:

$$\tau(T) = \tau_\infty \exp\left(\frac{B}{T-T_0}\right), \quad (5)$$

where τ_∞ represents the high–T limit of τ, and B and T_0 are material-specific parameters. Following common practice in molecular dynamics (MD) simulations, T_g is defined as the temperature at which τ reaches 1 ns. Using this criterion, the T_g of PS is determined to be ~371 K, while that of PMMA is ~401 K, and that of PVC is ~355 K.

In this work, we define intrinsic fragility (m) by:

$$m = \left(\frac{\partial \log_{10}\tau}{\partial\left(\frac{T_g}{T}\right)}\right)_{T=Tg} \quad (6)$$

A plot of $\log_{10}\tau$ verses T_g/T for PMMA, PS, and PVC is shown in Supplementary Fig. 6c. The computational results of m are presented in Table 2 and Supplementary Fig. 6d.

4. Instantaneous positions of atoms and the shear mode assumption

Two side-view snapshots of the slender model (Fig. 8c), taken at different times along the x and y axes for the three polymers are shown in Supplementary Fig. 8. The results show that the shear mode is approximately linear at the beginning of the simulation. As simulation progresses beyond ~100 ns, fluctuating noise gradually distorts the linear configuration of the model.

According to the shear mode assumption proposed in our previous publication[3], enhanced relaxations in the microscale surface region arise from spontaneous shear excitations involving an initial lateral displacement (ξ) and a vertical propagation distance (l), as illustrated in Supplementary Fig. 7a. By equating the energy of such an excitation, U, to $k_B T$, corresponding to spontaneous excitations, we derive:

$$U \approx \frac{1}{2}G\left(\frac{\xi}{l}\right)^2 \xi^2 l \approx k_B T, \quad (7)$$

which can be rearranged to give:

$$l \approx \frac{\xi^4 G}{2k_B T}. \quad (8)$$

Here, $G \approx 1$ GPa is the shear modulus of the polymer. By substituting $T = 300$ K and $\xi \sim 1$ nm, one finds that $l \sim 1$ μm. Although the exact value of the shear modulus varies slightly among the different polymers investigated, this simple equation demonstrates that short-range thermal excitations in nanoscale mobile layer can produce long-range shear modes extending up to micrometer scale.

We notice that the length scale of shear excitation, l, is proportional to the 4th power of ξ, making its value highly sensitive to the lateral displacement in different polymers. In the main text, we find that the average velocity field is strongest for PVC, followed by PS and PMMA (Fig. 5b). Consequently, the lateral displacement ξ is also the greatest for PVC, followed by PS and PMMA, resulting in the most penetrating shear mode for PVC compared to PS and PMMA (Supplementary Fig. 9b). In our simulation, the model's vertical dimension is restricted to 250 nm. Due to the significant molar mass applied to the substrate atoms, all shear mode displacements are terminated at the bottom. Under this circumstance, the gradient of lateral displacements along the z-axis can serve as an indicator of the strength of the shear mode (Supplementary Fig. 9a).

5. The diffusion displacement profile for determining h_t^{nano}

The profiles of σ_{diff} at $\Delta t = 0.8, 2.4, \text{and } 8.0$ ns are shown in Supplementary Fig. 10 (a to c). All profiles show an increase near the surface at $z = 0$. Although the value of σ_{diff} increases with Δt, the curves overlap after normalization with the bulk average (computed from the data in the range $50 < z < 150$ nm, which are not shown) (Supplementary Fig. 10 (d to f)). This result indicates that the trend of σ_{diff} is independent of Δt. In these normalized graphs, we observe that σ_{diff} decreases linearly near the surface. The intersection of the fitted linear line with $y = 1$ is calculated as the thickness of the nanoscale mobile layer.

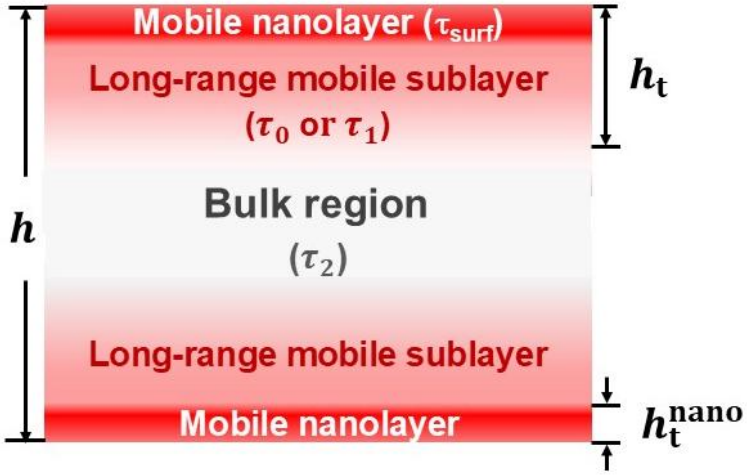

Supplementary Fig. 1 | Schematic showing the mobile surface bilayer structure within a free-standing film as well as symbols for the layer and film properties discussed in this paper.

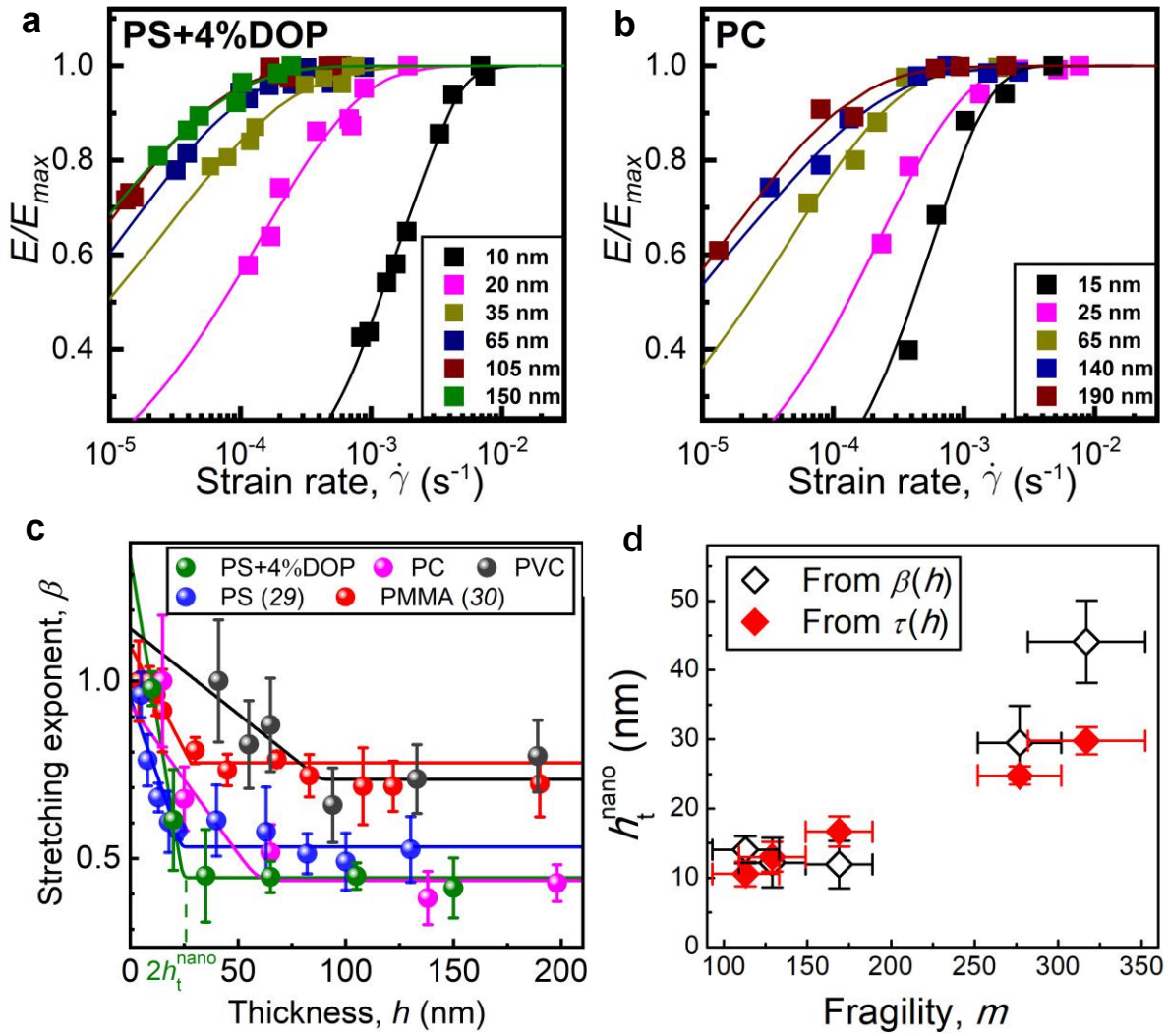

Supplementary Fig. 2 | Analysis from strain-rate dependent elastic measurements of the polymers studied. a-b Normalized elastic moduli for films of PS+4% DOP and PC, respectively, with varying thicknesses at room temperature. The solid lines represent best fits to Equation (1). **c** Plots of stretching exponent (β) versus film thickness (h) for the polymers studied. Error bars correspond to standard errors (SE) of β values obtained by fitting the data of Fig. 1a and panels **a** and **b** to Equation (1). Dashed lines indicate previously reported data for PS[29] and PMMA[30]. Available under a CC BY-NC 4.0 License. Copyright 2025, Nie et al. **c** Stretching exponent β plotted versus film thickness h for various polymers. **d** Surface nanolayer thickness h_t^{nano} plotted against fragility m, with data coming from different sources: open diamonds are extracted from **c** as the thickness at which β becomes independent of h; the red diamonds are obtained from Fig. 1b as the thickness below which τ_{film} becomes constant. The vertical error bars for h_t^{nano} "From $\tau(h)$" (open diamonds) represent the uncertainties presented in Table 1; those for h_t^{nano} "From $\beta(h)$" (solid diamonds) represent the SE derived from fitting the profiles in panel **c** to a function consisting of a slanted straight line and a horizontal straight line. The horizontal error bars indicate the uncertainties of the m values presented in Table 2. In all panels, each data point was derived from one set of measurements.

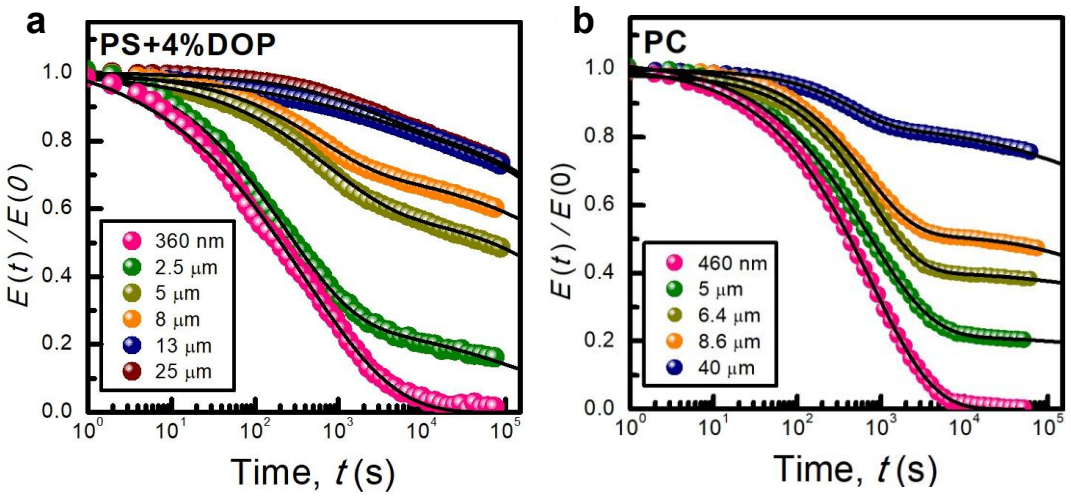

Supplementary Fig. 3 | Time dependence of the normalized relaxation moduli ($E(t)/E_0$) for **a** PS+4%DOP and **b** PC at a temperature of $0.89T_g$.

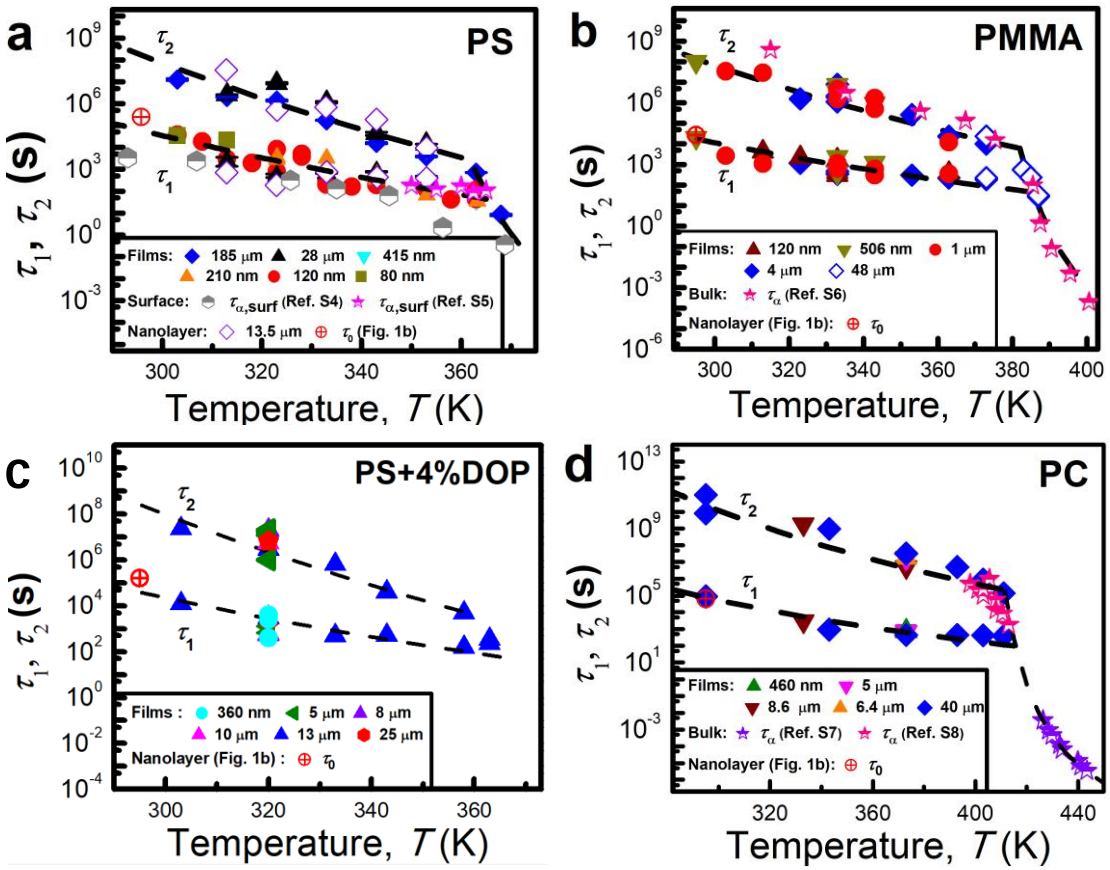

Supplementary Fig. 4 | Fast (τ_1) and slow (τ_2) relaxation times for films of various polymers as a function of temperature. The polymers include **a** PS, **b** PMMA, **c** PS+4%DOP, and **d** PC. The black dashed lines represent Arrhenius fits to the data of τ_1 and τ_2 at temperatures below T_g−10 K, as well as a Vogel-Fulcher-Tammann (VFT) fit (Supplementary Equation (5)) for τ_2 at temperatures above T_g−10 K. The values of τ_1 and τ_2 at room temperature (~295 K) for each polymer were obtained by extrapolating the Arrhenius fits of their temperature-dependent data to ~295 K. The structural relaxation times (τ_α) of the surface and the bulk, as reported in literature within a wide T range (half-filled symbols) if available, are included to demonstrate alignment with our findings. Among these data, Supplementary Reference 4 (Ref. S4 in **a**) was adapted with permission. Copyright 2008 by the American Association for the Advancement of Science. Supplementary Reference 5 (Ref. S5 in **a**) was adapted with permission. Copyright 2011 by The American Chemical Society. Supplementary Reference 6 (Ref. S6 in **b**) was adapted with permission. Copyright 1952, Elsevier Inc. Supplementary Reference 7 (Ref. S7 in **d**) was adapted with permission. Copyright 1966, Wiley Periodicals, Inc. Supplementary Reference 8 (Ref. S8 in **d**) was adapted with permission. Copyright 2001, by Elsevier Science Ltd.

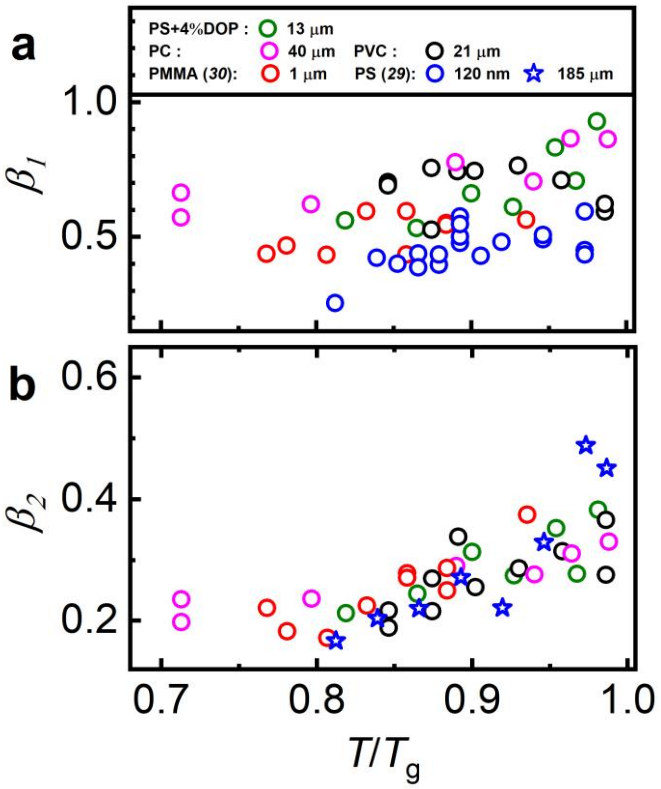

Supplementary Fig. 5 | Plots of β_1 (**a**) and β_2 (**b**) of the polymers studied as a function of temperature (T) normalized by the polymer's T_g.

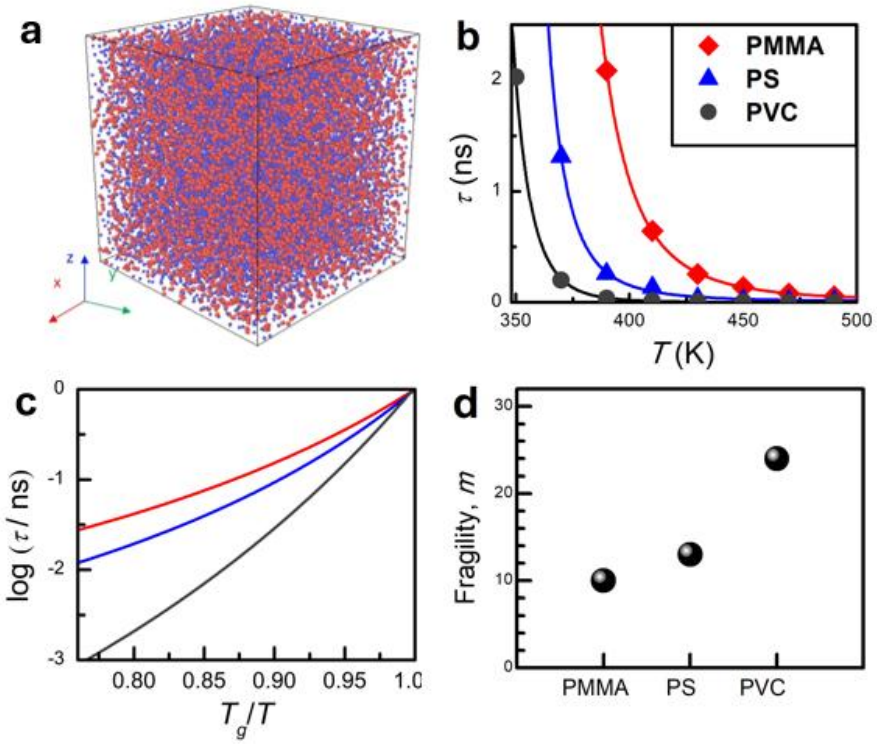

Supplementary Fig. 6 | Determination of fragility (m) for CG models of PMMA, PS, and PVC using their $\tau(T)$ data. a A representative bulk CG-model used to compute the structural relaxation time of the polymer system. **b** Plots of τ as a function of temperature T for various polymers. The solid lines represent the best fits to Supplementary Equation (5). **c** Data from **b** replotted as log τ verses T_g/T, where T_g refers to the $T_{g,CG}^{bulk}$ values listed in Table 2. **d** The computed fragility values for PMMA, PS and PVC, derived from the data in **c**.

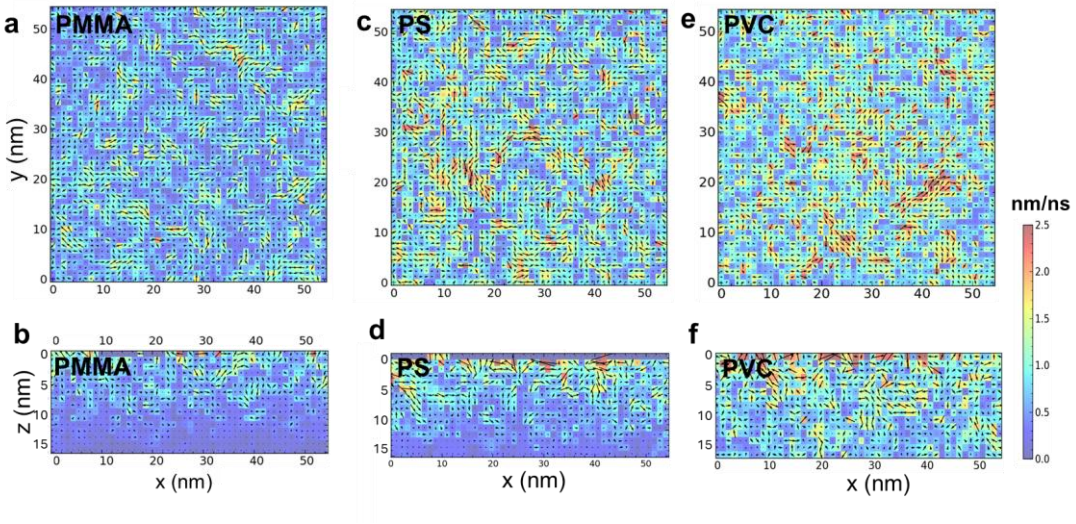

Supplementary Fig. 7 | The average velocity fields for the three polymers studied. The top panels show the x-y cross-sections at 1 nm below the top boundary, while the bottom panels show the x-z cross-sections at $y = 0$ of these fields. The previously published data for PMMA and PS [3] are available under a CC BY-NC 4.0 License. Copyright 2025, Nie et al.

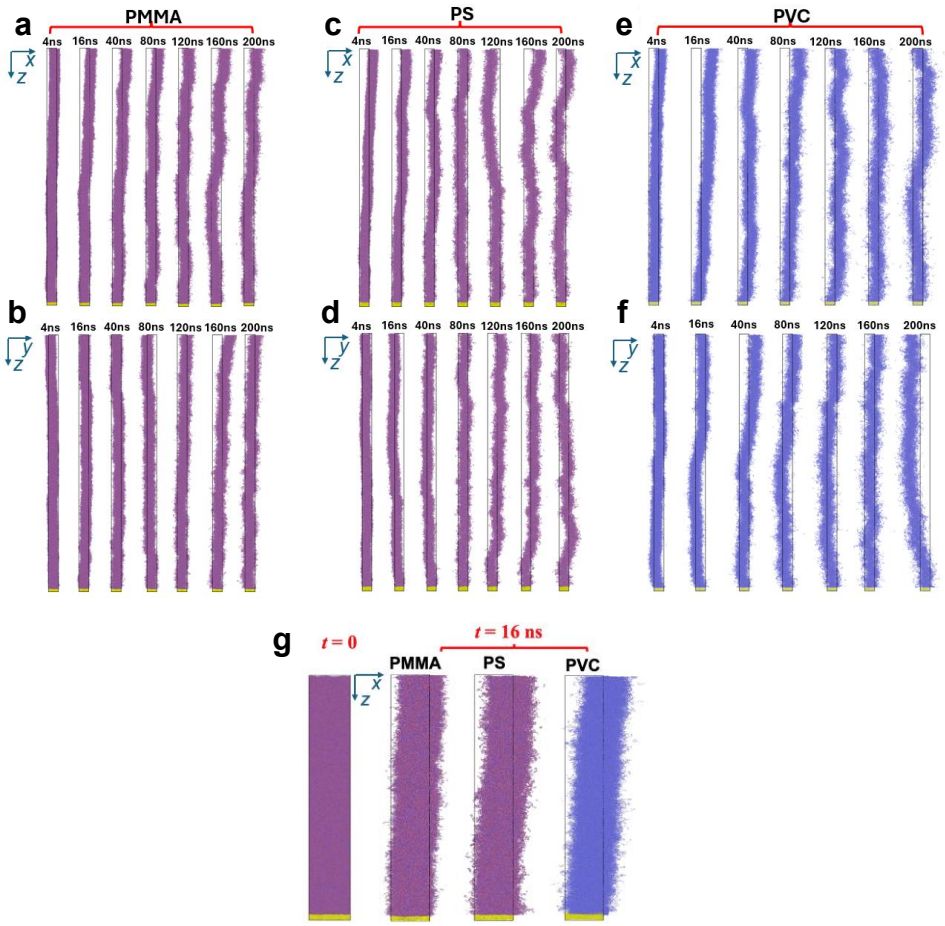

Supplementary Fig. 8 | Side-view snapshots of the slender model after various time intervals for three polymers. a–b Time evolution of the model for PMMA, viewed along the y (**a**) and x (**b**) axes. **c–d** Time evolution of the model for PS, viewed along the y (**c**) and x (**d**) axes. **e–f** Time evolution of the model for PVC, viewed along the y (**e**) and x (**f**) axes. **g** Results analogous to those in Fig. 6a are shown for t = 0 and 16 ns, using a slender model with twice the lateral dimensions (L_x and L_y) and half the thickness (L_z), under otherwise identical conditions.

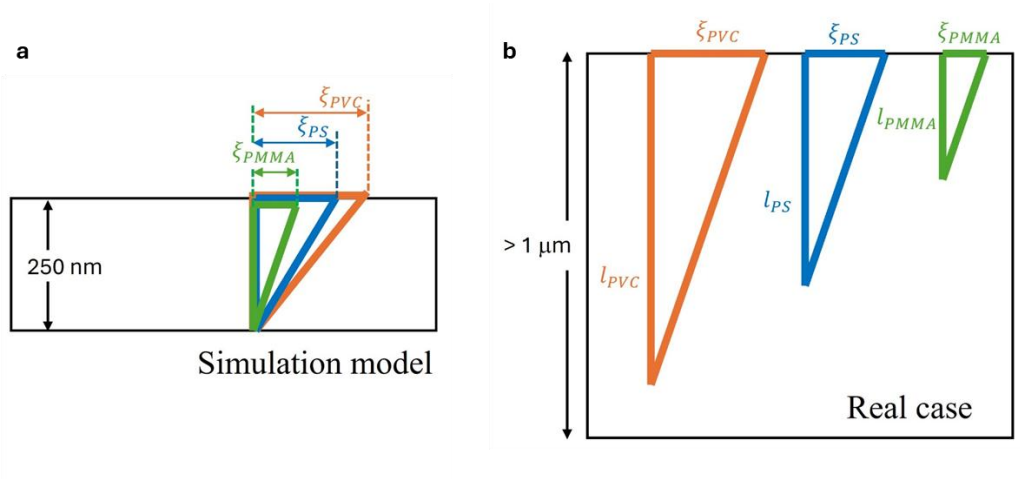

Supplementary Fig. 9 | Illustration of the center-of-mass (COM) displacement field in a shear excitation mode for the three simulated polymer models. a Simulation model: due to simulation constraints, the model thickness (h) is set to 250 nm, which is smaller than the intrinsic propagation distance (l) of the shear mode, causing the shear mode to terminate at the substrate. Consequently, the observed value of l equals the system thickness. **b** Experimental (real) case: the system thickness exceeds the intrinsic length of the longest shear mode. So, shear propagation terminates naturally before reaching the substrate. The assumption that $\xi \sim l$ aligns with the experimentally observed scaling between the surface relaxation rate and h_t or h_t^{nano} (Fig. 7c) and the simulated scaling between the surface velocity and h_t^{nano} (Fig. 7b).

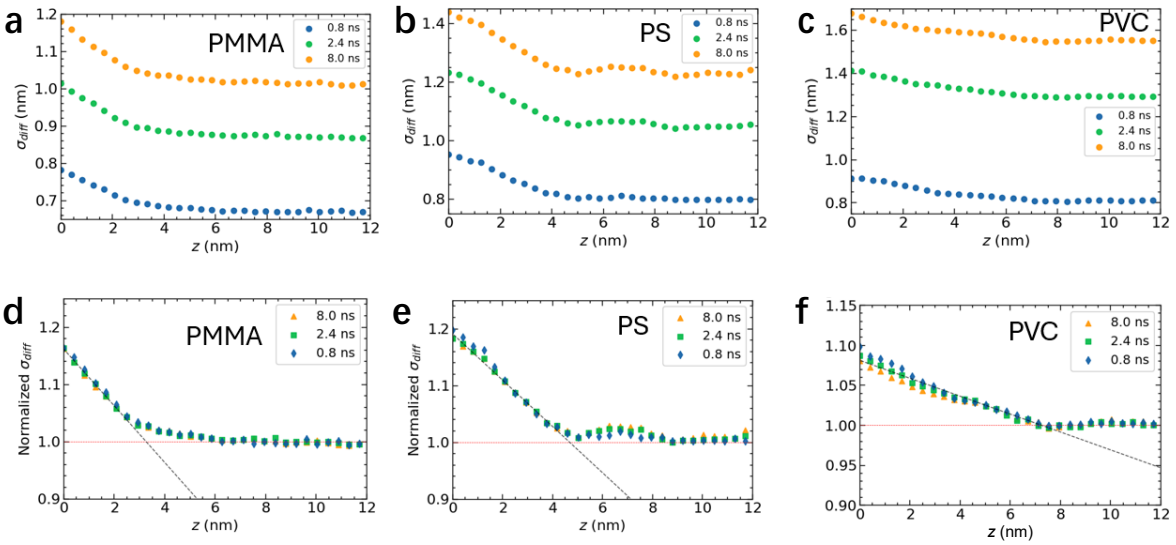

Supplementary Fig. 10 | Depth (z) profiles of the diffusive displacement (σ_{diff}) for the studied polymers. a–c The upper panels display the depth profiles of σ_{diff} at different times: 8.0, 2.4, and 0.8 ns for PMMA, PS, and PVC, respectively. **d–f** The lower panels show the same data normalized to the bulk value of σ_{diff} for the corresponding polymers. The black and red straight lines represent the best fits for the near-surface and bulk regions, respectively. In all panels, $z = 0$ indicates the position of the free surface.

PS+4%DOP:

h (nm)	E_{max} (GPa)
10	2.80 ± 0.13
20	2.86 ± 0.02
35	2.91 ± 0.02
65	3.00 ± 0.08
105	3.05 ± 0.02
150	3.03 ± 0.04

PC:

h (nm)	E_{max} (MPa)
15	2.11 ± 0.12
25	2.21 ± 0.14
65	2.29 ± 0.07
140	2.34 ± 0.08
190	2.38 ± 0.02

PVC:

h (nm)	E_{max} (MPa)
41	2.70 ± 0.09
65	2.84 ± 0.11
94	2.89 ± 0.08
133	2.93 ± 0.03
189	2.98 ± 0.05

Supplementary Table 1 | Lists of maximum elastic moduli (E_{max}) used to obtain the normalized data presented in Fig. 1a and Supplementary Figs. 2a, b. The samples are films of PS+4%DOP, PC and PVC and the temperature is 295 K. The uncertainties represent standard error (SE) of the E_{max} values, determined by fitting the E versus h data in the large-h region where the $E(h)$ plot reaches saturation.

Polymers	Monomer formula	# of atoms (all atoms)	# of heavy atoms	# of CG beads	mapping ratio
PVC	C_2H_3Cl	6	3	1	3:1
PS	C_8H_8	16	8	2	4:1
PMMA	$C_5H_8O_2$	15	7	2	3.5:1

Supplementary Table 2 | Mapping ratios of PVC, PS and PMMA.

Supplementary References

1. Kwansa AL*, et al.* Molecular mechanism of plasticizer exudation from polyvinyl chloride. *Macromolecules* **56**, 4775-4786 (2023).

2. Fulcher GS. Analysis of recent measurements of the viscosity of glasses. *J Am Ceram Soc* **8**, 339-355 (1925).

3. Nie H, Chen X, Ma Z, Zhang R, Tsui OK. Exploring Long-Range Surface-Induced Mobility Enhancement in Poly (methyl methacrylate). *Macromolecules* **58**, 10937-10947 (2025).

4. Fakhraai Z, Forrest JA. Measuring the Surface Dynamics of Glassy Polymers. *Science* **319**, 600-604 (2008).

5. Paeng K, Swallen SF, Ediger MD. Direct Measurement of Molecular Motion in Freestanding Polystyrene Thin Films. *J Am Chem Soc* **133**, 8444-8447 (2011).

6. McLoughlin JR, Tobolsky AV. The viscoelastic behavior of polymethyl methacrylate. *J Colloid Sci* **7**, 555-568 (1952).

7. Matsuoka S, Ishida Y. Multiple Transitions in Polycarbonate. *J Polym Sci, Part C: Polym Symp* **14**, 247-259 (1966).

8. Heymans N, Dequenne B. Relationship between conformation and enthalpy or volume relaxation in polycarbonate. *Polymer* **42**, 5337-5342 (2001).